Optical properties of the neutral silicon split-vacancy center in diamond

U. F. S. D'Haenens-Johansson, A. M. Edmonds, B. L. Green, and M. E. Newton*
Department of Physics, University of Warwick, Coventry, CV4 7AL, United Kingdom

G. Davies
Department of Physics, King's College London, Strand, London, WC2R 2LS, United Kingdom

P. M. Martineau and R. U. A. Khan
DTC Research Centre, Belmont Road, Maidenhead, Berkshire, SL6 6JW, United Kingdom

D. J. Twitchen
Element Six Ltd., King's Ride Park, Ascot, Berkshire, SL5 8BP, United Kingdom

(Received 1 March 2011; revised manuscript received 6 November 2011; published 21 December 2011)

The zero-phonon line (ZPL) at 1.68 eV has been attributed to the negatively charged silicon split-vacancy center in diamond, (Si-V)$^-$, and has been extensively characterized in the literature. Computational studies have predicted the existence of the neutral charge state of the center, (Si-V)^0, and it has been experimentally observed using electron paramagnetic resonance (EPR). However, the optical spectrum associated with (Si-V)^0 has not yet been conclusively identified. In this paper the 1.31 eV band visible in luminescence and absorption is attributed to (Si-V)^0 using an approach which combines optical absorption and EPR measurements. The intensities of both 1.68 eV and 1.31 eV bands are found to increase in deliberately Si-doped chemical vapor deposition (CVD) grown diamond, and also after electron irradiation and annealing, suggesting the involvement of both Si and a vacancy in the centers. The 1.31 eV ZPL is unambiguously associated to Si by its shift to a lower energy when the dominant Si isotope is changed from ^{28}Si to ^{29}Si. Charge transfer between (Si-V)$^-$ and (Si-V)^0 induced via ultraviolet photoexcitation or heating in the dark allows calibration factors relating the integrated absorption coefficient of their respective ZPLs to the defect concentration to be determined. Preferential orientation of (Si-V)^0 centers in CVD diamond grown on {110}-oriented diamond substrates is observed by EPR. The (Si-V)^0 centers are shown to grow predominantly into CVD diamond as complete units, rather than by the migration of mobile vacancies to substitutional Si (Si$_S$) atoms. Corrections for the preferential alignment of trigonal centers for quantitative analysis of optical spectra are proposed and the effect is used to reveal that the 1.31 eV ZPL arises from a transition between the $^3A_{2g}$ ground state and $^3A_{1u}$ excited state of (Si-V)^0. A simple rate equation model explains the production of (Si-V)^0 upon irradiation and annealing of Si-doped CVD diamond. In as-grown Si-doped diamond the (Si-V) defects only account for a fraction of the total silicon present; the majority being incorporated as Si$_S$. The data show that both Si$_S$ and (Si-V) are effective traps for mobile vacancies.

DOI: 10.1103/PhysRevB.84.245208 PACS number(s): 81.05.ug, 78.40.Fy, 78.55.Ap, 76.30.Mi

I. INTRODUCTION

The presence of silicon (Si) in diamond has been routinely verified by the detection of the 1.68 eV (737 nm) zero-phonon line (ZPL) in luminescence or absorption, which has been attributed to the negatively charged silicon split-vacancy center, (Si-V)$^-$.[1,2] Unless preventative measures are taken, Si impurities may be introduced into chemical vapor deposition (CVD) grown diamond as a consequence of plasma etching of Si-containing reactor components.[3,4] Intentional Si-doping has been achieved during the growth of both CVD and high-pressure, high-temperature (HPHT) synthetic diamond.[5,6] The occurrence of (Si-V)$^-$ in natural untreated diamond is rare. Of the order of 1 in 1000 gem-quality specimens investigated by a major grading laboratory contain this center.[7,8] Therefore, observation of (Si-V)$^-$ is frequently used to help distinguish between natural, CVD synthetic or treated diamond.[7,8]

There has also been interest in (Si-V)$^-$ by the quantum-information community due to its potential use as a single photon source. Single photon detection from color centers in diamond has been achieved using the negatively charged nitrogen-vacancy [(N-V)$^-$] center,[9,10] with its ZPL at 1.945 eV (637 nm), and systems with ZPLs at 1.55 eV (802 nm)[11,12] and 1.64 eV (756 nm).[13] Most research has been conducted on (N-V)$^-$ due to its long coherence time and the relative ease of fabrication.[14] However, its broad emission band at room temperature is a disadvantage as it prevents efficient filtering of the background signals.[10] Room temperature single photon emission has been observed from (Si-V)$^-$ centers in ion implanted type IIa bulk diamond[15] and more recently with a much greater quantum efficiency in Si-doped CVD nanodiamonds.[16] There are several properties that render (Si-V)$^-$ noteworthy for quantum-information applications. (Si-V)$^-$ has a remarkably sharp ZPL, with a width of ∼0.7 nm reported at room temperature (to date, the most narrow for a color center in diamond),[16] and a weak vibronic sideband characterized by a small Huang-Rhys factor S_{HR}. The values of S_{HR} for the 1.68 eV band of the (Si-V)$^-$ center determined from both absorption and photoluminescence measurements cited in the literature range from 0.05 to 0.29.[16–19] Furthermore, the centers emit light in a wavelength region where there is low background fluorescence from diamond.[16] Recent reports of single photon count rates up to 4.8×10^6 counts/s at saturation for (Si-V)$^-$ are significantly higher than those for

 ©2011 American Physical Society

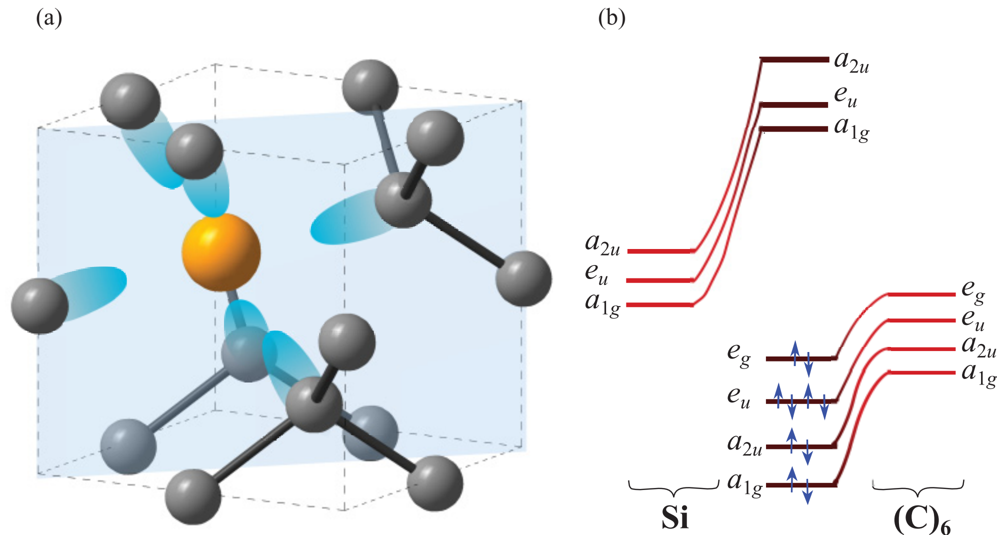

FIG. 1. (Color online) (a) Schematic of the silicon split-vacancy defect in diamond, (Si-V), with the {110} mirror plane highlighted. The silicon atom is illustrated as a large yellow sphere lying halfway between two vacant lattice sites; all other atoms are carbon, with the dangling orbitals shown in blue. The silicon atom is equidistant from six nearest-neighbor carbon atoms. (b) Simple molecular-orbital model for (Si-V): The central silicon atom and ligand orbitals interact, resulting in the molecular orbitals illustrated. The arrows indicate the 10 unpaired electrons available to fill the energy levels for $(\text{Si-V})^0$.

$(\text{N-V})^-$ ($\sim 10^5$ counts/s) and even the 1.64 eV luminescent center (3.2×10^6 counts/s).[10,13,16]

Electron paramagnetic resonance (EPR) and computational studies have shown the existence of the neutral charge state of the silicon split-vacancy center $(\text{Si-V})^0$.[2,20,21] Although the center has been identified, its optical spectrum has not hitherto been unambiguously determined. The ZPL at 1.31 eV (946 nm) has been previously attributed to $(\text{Si-V})^0$ via a combination of EPR and optical absorption data.[22] Additionally, charge transfer was induced between the $(\text{Si-V})^-$ and $(\text{Si-V})^0$ centers, enabling the calculation of calibration factors which can be used to determine the concentration of the centers from the integrated absorption coefficients of the ZPLs at 77 K.[22] In this paper the optical properties of the 1.31 eV band are investigated in detail and new data are presented supporting the assignment to the $(\text{Si-V})^0$ center. Studies of the production of both the 1.68 eV and 1.31 eV bands by irradiation and annealing is modeled in terms of vacancy capture by substitutional silicon. Grown-in $(\text{Si-V})^0$ centers are shown by EPR to display preferential alignment with respect to the growth plane in homoepitaxial CVD diamond grown on {110}-oriented substrates. The importance of allowing for the preferential alignment of the centers when using optical absorption for quantitative measurements of the concentration of $(\text{Si-V})^0$ is demonstrated. It will be shown (Sec. IV B) that information about the nature of the 1.31 eV band transition can be extracted from measurements on samples in which the defect is preferentially aligned.

A. The silicon split-vacancy center in diamond

Spin-polarized local density-functional-cluster theory was employed by Goss *et al.* to predict that an impurity complex consisting of a substitutional silicon atom next to a vacant lattice site in diamond is unstable.[2] The system spontaneously relaxes into a split-vacancy configuration, with the silicon atom lying in a bond-centered site between two vacancies, with D_{3d} symmetry [Fig. 1(a)]. This configuration is also known as a paired or double semivacancy[23] and is consistent with the structure assumed by complexes in diamond which contain vacancies and large dopants, such as cobalt or nickel.[24–28]

A simple molecular orbital, similar to that used for a tin atom at the center of a divacancy in silicon,[29] can be used to interpret the electronic structure of the (Si-V) defect in diamond. The central silicon atom's $3s$ and $3p$ orbitals interact with the ligand orbitals which are formed from a linear combination of a single dangling orbital from each of the six carbon atoms. In D_{3d} symmetry the linear combination of carbon dangling orbitals transform as a_{1g}, a_{2u}, e_u, and e_g, while those for the silicon $3s$ and $3p$ transform as a_{1g}, and a_{2u} and e_u, respectively. Figure 1(b) shows that in this model the populated electronic orbitals derive primarily from the "divacancy" ligand orbitals of the six carbon atoms,[30] which have been lowered in energy by the presence of the silicon atom. Only a small admixture of silicon character is expected.

For $(\text{Si-V})^0$ 10 electrons are accommodated in these orbitals. The lowest energy configuration is $a_{1g}^2 a_{2u}^2 e_u^4 e_g^2$ [assuming the order of the orbital energy levels shown in Fig. 1(b)]. This one-electron configuration gives rise to ${}^3A_{2g}$, ${}^1E_g$, and ${}^1A_{1g}$ many-electron states. The spin triplet ${}^3A_{2g}$ state has been assigned to the observed $S = 1$ ground state of $(\text{Si-V})^0$, where S is the effective spin.[21] Promotion of an electron from e_u to e_g results in the configuration $a_{1g}^2 a_{2u}^2 e_u^3 e_g^3$, giving rise to the many-electron states ${}^3A_{1u}$, ${}^1A_{1u}$, ${}^3A_{2u}$, ${}^1A_{2u}$, ${}^3E_u$, and ${}^1E_u$. Another electron promotion results in an $a_{1g}^2 a_{2u}^2 e_u^2 e_g^4$ configuration and gives rise to ${}^3A_{2g}$, ${}^1E_g$, and ${}^1A_{1g}$ many-electron states. We would expect other configurations to be significantly higher in energy. Determining the order of the many-electron states from even the three configurations considered above is a taxing theoretical problem, and this is not attempted here, though

TABLE I. Summary of sample properties and treatments. For the samples that were irradiated, each irradiation treatment was followed by annealing according to the tabulated details.

	Sample A	Sample C	Sample D
Substrate orientation	{110}	{113}	{001}
^{29}Si abundance	90%	4.7%	4.7%
1st treatment	N/A	1×10^{18} 1.5 MeV e$^-$/cm^2 + 4 h anneal at 900 °C	1×10^{17} 1.5 MeV e$^-$/cm^2 + 4 h anneal at 900 °C
2nd treatment	N/A	N/A	5×10^{17} 1.5 MeV e$^-$/cm^2 + 4 h anneal at 900 °C
1st anneal	1 h at 1200 °C	N/A	N/A
2nd anneal	1 h at 1400 °C	N/A	N/A
3rd anneal	1 h at 1600 °C	N/A	N/A
4th anneal	2 h at 2000 °C	N/A	N/A

possible electron dipole transitions from the $^3A_{2g}$ ground state are considered. For the divacancy system of D_{3d} symmetry the components of the electron dipole operator, which are proportional to x, y, z, transform as follows: $z \subset A_{2u}$; $x,y \subset E_u$. Therefore, the allowed electron dipole transitions from the ground state are $^3A_{2g} \rightarrow {}^3A_{1u}$ and $^3A_{2g} \rightarrow {}^3E_u$.[30] The fact that the $^3A_{2g} \rightarrow {}^3A_{1u}$ and $^3A_{2g} \rightarrow {}^3E_u$ transitions have different polarization behavior is crucial later (Sec. IV B) to understand the nonrandom orientations of (Si-V) grown into samples.

In the negative charge state (Si-V)$^-$, there are 11 electrons to accommodate, giving rise to the lowest energy configuration $a_{1g}^2 a_{2u}^2 e_u^4 e_g^3$. A ^2E_g ground state is expected, and since the promotion of one electron from e_u to e_g gives rise to the ^2E_u state the 1.68 eV optical transition associated with (Si-V)$^-$ has been assigned to the $^2E_g \rightarrow {}^2E_u$ transition.[1,2] The band was shown to consist of a 12-line fine structure by Clark *et al.*,[1] where the 12 lines were divided into three groups of four equally intense lines, whose relative intensities reflected the relative abundance of the silicon isotopes (^{28}Si, ^{29}Si, and ^{30}Si). The multiplicity of the lines was consistent with a transition from an orbitally twofold degenerate ground state, split by 0.20 meV, to a doublet state split by 1.07 meV.[1] The splitting of the doublets has been attributed to a (dynamic) Jahn-Teller effect.[2] Despite the prediction that (Si-V)$^-$ has a paramagnetic ground state with $S = \frac{1}{2}$,[2,31] it has not yet been unambiguously observed using EPR.

II. EXPERIMENTAL DETAILS

A suite of single crystal samples grown homoepitaxially by microwave-assisted CVD on {110}, {001}, and {113}-oriented single crystal substrates (samples A, B, and C, respectively) were studied. All samples were intentionally doped with silicon by adding silane to the CVD growth gases; samples A and B were grown with 90% ^{29}Si-enriched silane (Voltaix USA), whereas samples C and D were grown using silane containing the natural abundance of Si isotopes (^{28}Si:^{29}Si:^{30}Si = 92.3:4.7:3.0). Sample D was grown on a {001}-oriented substrate and during growth the concentration of silicon in the gas phase was adjusted to produce a sample with six layers with progressively higher silicon doping. For samples A, B, and C the substrates were removed to leave free-standing plates, which were cut and polished to eliminate poor quality material from the edges. A cross-sectional piece of sample D was prepared, allowing the study of the different layers. Sample B was investigated in its as-grown state, while the other samples were treated by irradiation (samples C and D) and annealing (samples A, C, and D). The treatment histories of these samples are summarized in Table I. Anneals at temperatures of 1600 °C and below were carried out in forming gas (96% argon and 4% hydrogen) at atmospheric pressure and the anneal at 2000 °C occurred under a stabilizing pressure of 6 GPa. The concentration of silicon split-vacancy complexes was increased in samples C and D by treatments consisting of irradiation with 1.5 MeV electrons followed by annealing for 4 h at 900 °C. At 900 °C isolated vacancies are highly mobile (activation energy is 2.3 ± 0.2 eV)[32] and it is expected that after annealing for 4 h their concentration would be reduced to approximately zero. The fate of the vacancies depends on the nature and concentration of impurities and/or sinks (e.g., extended defects) in the diamond. In the absence of traps or sinks for the vacancies multivacancy clusters could be produced. Any substitutional silicon atoms present in the starting material could trap a mobile vacancy, producing additional (Si-V) centers. The relative concentration of (Si-V)^0 and (Si-V)$^-$ depends on the concentration of donors (such as neutral single substitutional nitrogen $N_S{}^0$) and defects which act as electron acceptors. The donor and acceptor defect concentrations may also change upon annealing. Before and after each treatment the samples were cleaned in boiling sulfuric acid supersaturated with potassium nitrite. EPR, photoluminescence (PL), and visible and near-infrared (visible/NIR) absorption spectroscopy studies were performed.

A commercial Bruker 9.7 GHz (X-band) spectrometer equipped with a Super-High Q (ER4122SHQ) cavity was used for room temperature EPR measurements. The system was set up so that it was possible to rotate the sample in two perpendicular planes. The average concentrations of (Si-V)^0 were determined by EPR. Microwave power saturation, which occurs when the spin lattice relaxation rate is not sufficiently high to maintain the equilibrium spin population distribution while stimulated transitions are excited by microwaves, needs to be considered if EPR is to be used in a quantitative manner. Spectra were collected at several different powers to verify that microwave power saturation was not occurring.

The spectrometer was run using magnetic field modulation such that the spectral features approximate the first derivative of the EPR line shape. The EPR intensity was determined by fitting the experimental spectrum to a simulated spectrum, deconvolving overlapping spectra from different defects, and integrating the latter twice using a computer program developed in-house. A Tsallis function was used to produce the simulated spectra since EPR line shapes are usually not well reproduced with Lorentzian or Gaussian functions.[33] Furthermore, the algorithm utilizes the pseudomodulation technique to account for the distortion of the EPR line shape due to field modulation. Defect concentrations were calculated by comparing the EPR signal intensities to that of a reference sample of known concentration. The reference sample used in this study is a small, single growth sector, HPHT synthetic Ib diamond containing 270 ± 20 ppm atoms of N_S^0 (1 ppm = 1 part per million carbon atoms = spin density of 1.76×10^{17} cm^{-3}).

PL measurements were performed on a Renishaw Raman InVia microscope system equipped with an Oxford Instruments LHe Microstat cryostat for low temperature experiments. Measurements were made using 514 nm (2.410 eV) and 785 nm (1.579 eV) excitations, provided by an argon-ion laser and a solid-state laser, respectively. A PerkinElmer Lambda 1050 spectrophotometer furnished with an Oxford Instruments Optistat continuous flow helium cryostat was utilized to acquire visible/NIR absorption spectra at temperatures between 4 K and room temperature.

The average total silicon concentration in each ∼200-μm thick layer of sample D was determined by secondary ion mass spectrometry (SIMS). The experiments were carried out in a Cameca IMS 3F using $^{18}O_2^+$ bombardment and positive secondary ion detection to optimize the sensitivity to silicon. In order to minimize sample charging effects the sample was coated with a thin layer of gold, which was subsequently sputtered away in the region of interest by rastering over an area nominally 200 μm across. The raster was then collapsed to a spot and measurements were taken every 50 μm. Five of the six layers were found to be homogeneous, to within the uncertainty of the measurement (±10%). However, the final growth layer, which contained the highest silicon concentration (∼ 1.4 ppm), was inhomogeneously doped.

Thermochromic and photochromic changes in the charge states of defects were investigated. The samples were illuminated for ∼2 min with 224 nm (5.54 eV) light from a Photon Systems AgHe laser (the indirect band gap of diamond[34] is 5.48 eV). The peak laser power was ∼100 mW, the pulse duration ∼75 μs, and the pulse frequency 20 Hz. Sample heating was conducted at 850 ± 10 K for 20 min in a Carbolite tube furnace in the dark. When the treatment was complete the sample was quickly removed from the furnace and quenched to room temperature in water. After the heating treatment further sample handling was conducted in the dark and care was taken to avoid exposure to ultraviolet (UV) excitation. Before and after each treatment the average concentrations of $(\text{Si-V})^0$ and N_S^0 were measured using EPR. Additionally, visible/NIR absorption spectra were collected to monitor any changes to the optical spectra.

III. RESULTS

A. Optical absorption and PL

Both the 1.31 eV and 1.68 eV $[(\text{Si-V})^-]$ bands were detected in all samples using PL and optical absorption. A typical absorption spectrum at 77 K is illustrated in Fig. 2(a). The features observed at 1.447 ± 0.001 eV and 1.493 ± 0.002 eV have previously been reported in silicon-containing diamond.[22,35] The intensities of these features were found to correlate with the intensity of the 1.31 eV peak by

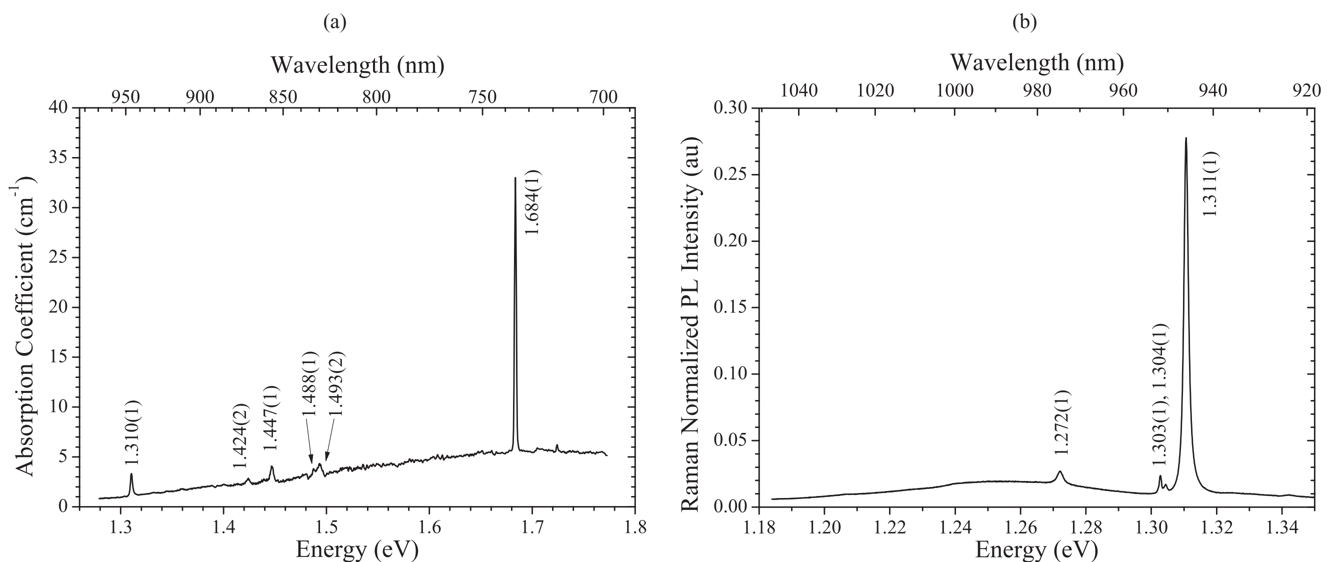

FIG. 2. (a) NIR absorption and (b) PL spectra of sample A (after annealing at 2000 °C), taken at 77 K. In the absorption spectrum the peaks at 1.447 ± 0.001 eV and 1.493 ± 0.002 eV related to the photoconductivity threshold at 1.5 eV are visible.[35] The photoconductivity produces a rise in absorption which partially obscures the vibronic band of the 1.310 ± 0.001 eV feature. Vibronic structure can be resolved in the PL spectrum, though it is noteworthy that the data have not been corrected for the detector response, which decreases with decreasing energy and so may reduce the apparent size of the band.

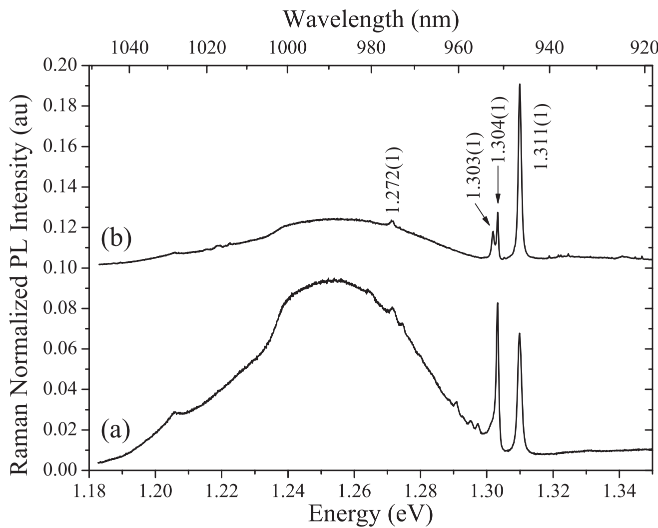

FIG. 3. Raman-normalized PL spectra measured at 5 K of sample A when it was (a) as-grown and (b) annealed at 2000 °C. The 1.31 eV feature was visible in both absorption and PL; all other labeled features were not detected in absorption.

Allers and Collins.[35] The result was explained by attributing the peaks to transitions to excited states of the same defect giving rise to the photoconductivity threshold at 1.5 eV.[35] The optical transitions that produce the photoconductivity result in a rise in absorption, possibly obscuring the vibronic band of the 1.31 eV ZPL. At 77 K the 1.310 ± 0.001 eV and 1.684 ± 0.001 eV peaks dominated the optical absorption spectra up to the band edge energy.

Figure 2(b) shows a PL spectrum recorded with 785-nm excitation at 77 K. The spectrum has not been corrected for the response function of the silicon CCD detector used in this spectrometer. The features at 1.272 ± 0.001 eV, 1.303 ± 0.001 eV, and 1.304 ± 0.001 eV were not observed in absorption. To aid the comparison of different PL spectra, they have been normalized to the integrated intensity of the diamond Raman peak. In this figure, and those that follow, they are referred to as Raman-normalized PL spectra.

Figure 3 shows the Raman-normalized PL spectra (785-nm excitation, 5 K) for sample A, in its as-grown state [Fig. 3(a)] and after annealing at 2000 °C [Fig. 3(b)]. The intensities of the 1.304 eV and 1.31 eV bands do not correlate in different samples and so these features cannot originate from the same defect. The broad emission band centered on ∼1.25 eV appears to correlate with the ZPL at 1.304 eV and is thus associated with its vibronic band. The vibronic coupling in the 1.304 eV system is strong, and overlaps with the vibronic band of the 1.31 eV system, making measurement of this band very difficult.

Inspection of the PL spectra shown in Figs. 2(b) and 3(b) reveals that between 77 K and 5 K the intensity of the 1.31 eV ZPL falls significantly and the relative intensity of the 1.303 eV and 1.304 eV peaks changes. To investigate the vibronic coupling of the 1.31 eV system the temperature variation of the integrated intensity of its ZPL was measured in absorption and PL for sample A (after it was annealed at 2000 °C); the resulting data are shown in Fig. 4. The experimental data are shown by points and the lines were calculated as described in Sec. IV A.

The defect associated with the 1.31 eV ZPL was unambiguously confirmed to be silicon related by comparing the peak energies in absorption of the 1.31 eV and 1.68 eV bands at 4 K in samples containing ^{29}Si-isotopic abundances of either 4.7% (sample C) or 90% (samples A and B). Both ZPLs were found to decrease in energy by on average 0.4 ± 0.1 meV when the dominant silicon isotope changed from ^{28}Si to ^{29}Si (Fig. 5).

B. EPR

(Si-V)^0 concentration measurements were made using EPR, where it was noted that for sample A (as-grown) the relative intensities of the resonance lines changed depending on whether the magnetic field, $\boldsymbol{B}$, was aligned parallel to a crystallographically equivalent direction lying in or out of

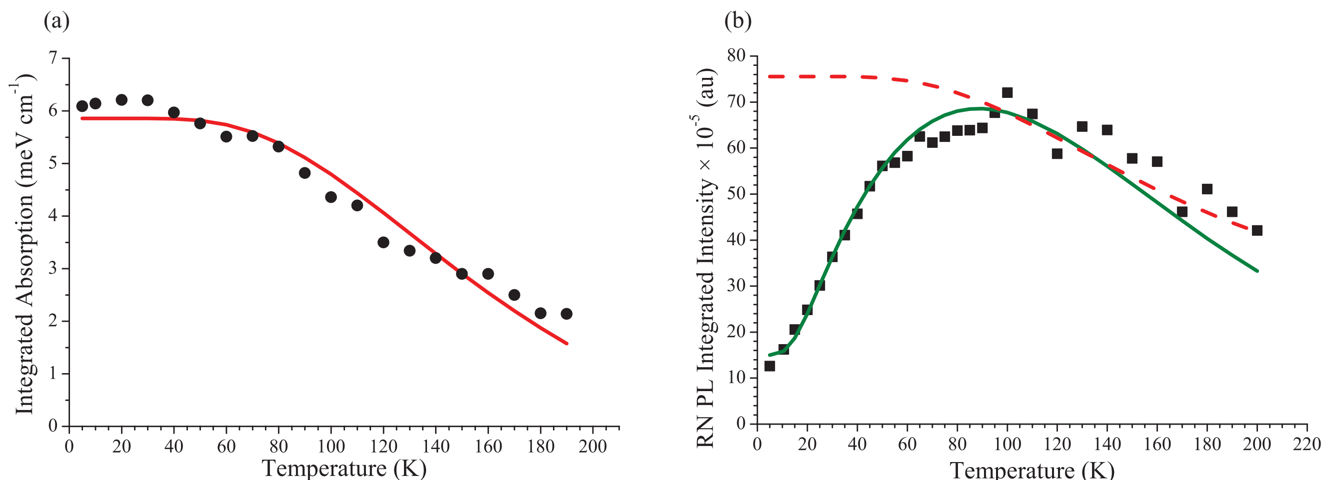

FIG. 4. (Color online) (a) Integrated absorption coefficient of the 1.31 eV ZPL as a function of the sample temperature. The solid curve is the best fit to the data using Eq. (1). (b) Temperature variation of the 1.31 eV ZPL Raman-normalized PL integrated intensity, measured using 785-nm excitation. The broken curve shows the variation in the absorption and is for comparison only. The solid line is the best fit of the data to Eq. (2). Uncertainties on the integrated absorption and the Raman-normalized PL integrated intensity measurements are estimated to be ±10%. These experiments were made using sample A after it had been annealed at 2000 °C.

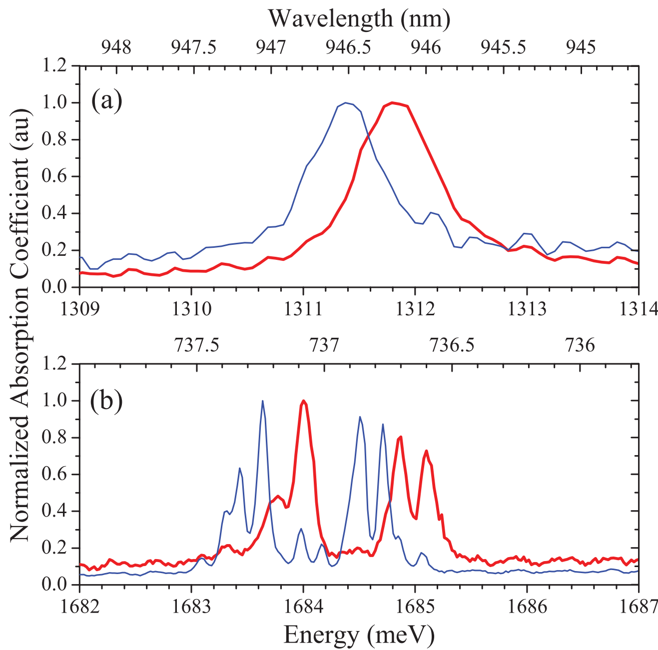

FIG. 5. (Color online) Visible/NIR absorption spectra obtained at 4 K for samples B (thin, blue line) and C (thick, red line), which have ^{29}Si isotopic abundances of 90% and 4.7%, respectively. The spectral intensities have been normalized to the maximum height of the each band to facilitate comparison. The (a) 1.31 eV and (b) 1.68 eV bands shift to a lower energy by 0.4 ± 0.1 meV when the ^{29}Si abundance was increased.

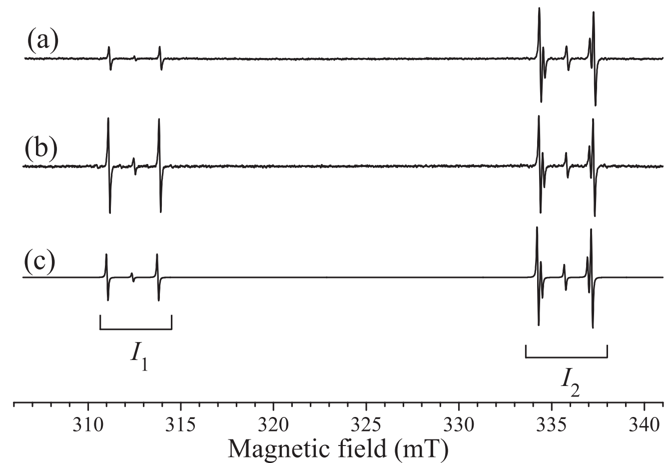

FIG. 6. EPR spectra of (Si-V)^0 at X-band frequencies for the as-grown sample A with the magnetic field aligned parallel to the (a) $[\bar{1}1\bar{1}]$ or (b) [111] directions, where the growth plane is assumed to be (110). The former direction lies in the growth plane while the other lies out of the growth plane. The difference in the relative resonance line intensities of the spectra is attributed to the preferential alignment of the centers in this sample. If the centers were statistically aligned along each crystallographically equivalent direction the resulting spectra would look like the simulated spectrum (c).

the {110} growth plane. The EPR spectra acquired for the as-grown sample A with $\boldsymbol{B} \parallel \langle 111 \rangle$ are shown in Fig. 6. If the (Si-V)^0 centers in a sample were statistically aligned with their $\langle 111 \rangle$-symmetry axes along all crystallographically equivalent directions the resulting spectrum would look like the simulated spectrum [spectrum (c) in Fig. 6]. The spectrum was simulated using the Hamiltonian parameters published by Edmonds *et al.*[21]

The integrated absorption of the 1.31 eV ZPL was correlated with the (Si-V)^0 concentration in the samples, as measured using EPR. To ensure that charge transfer between (Si-V)^0 and (Si-V)$^-$ was not induced during the experiments the samples were not exposed to UV light during the EPR measurements. Subsequently, sample handling was carried out in the dark and optical absorption spectra were recorded using monochromatic light, starting at low ($<$1.29 eV) energies and finishing at $\sim$1.7 eV. Figure 7 shows the integrated absorption of the 1.31 eV ZPL plotted against the concentration of (Si-V)^0 measured by EPR in a variety of samples. Some of the data points are from samples treated (UV photoexcitation or heating in the dark) to change the relative concentration of (Si-V)^0 and (Si-V)$^-$.[22] The graph also includes data from samples where EPR measurements indicated that the (Si-V)^0 defects were not randomly oriented. The analysis required to correct for the preferential alignment is discussed in Sec. IV B.

C. Electron irradiation and annealing studies

In order to confirm that the center responsible for the 1.31 eV band involved both a vacancy and a silicon atom, the layered sample (D) was irradiated with 1.5 MeV electrons to a dose of 1×10^{17} cm^{-2} and annealed at 900 °C for 4 h. The PL intensities of both the 1.31 eV (using 785-nm excitation) and 1.68 eV (using 514-nm excitation) features were observed to increase in each layer of the sample as seen in Fig. 8. The sample was subjected to a second irradiation and annealing treatment, with the irradiation dose increased to 5×10^{17} 1.5 MeV electrons cm^{-2}. The 1.31 eV PL peak was seen to further

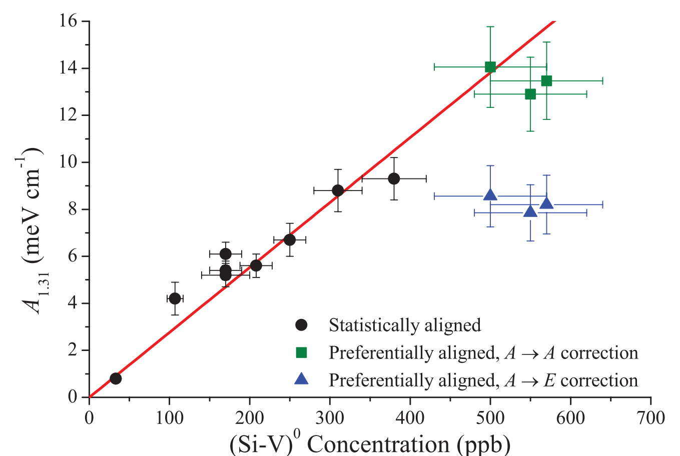

FIG. 7. (Color online) Correlation between the integrated absorption coefficient of the 1.31 eV ZPL (recorded at 77 K) and the concentration of (Si-V)^0 as determined by EPR. The black circles represent data for samples where the (Si-V)^0 centers are statistically aligned. The remaining data points were recorded for samples where the (Si-V)^0 centers exhibited a degree of preferential alignment, which could be quantified using EPR. The effect of preferential alignment on the absorption measurements has been corrected assuming that the 1.31 eV band is produced by either an $A \rightarrow A$ transition (green squares) or an $A \rightarrow E$ transition (blue triangles).

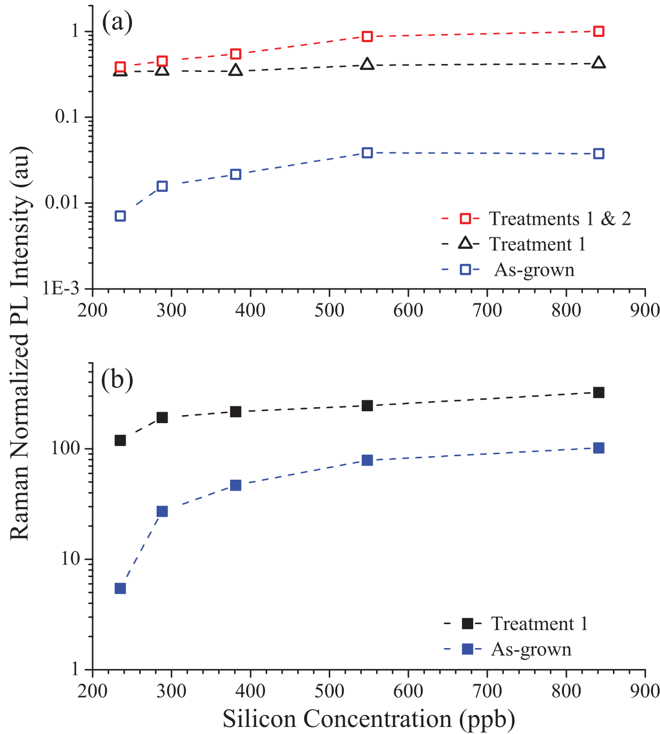

FIG. 8. (Color online) Raman-normalized PL intensity of the (a) 1.31 eV and (b) 1.68 eV zero-phonon lines as a function of silicon concentration in a sample D consisting of layers with different Si-doping levels. The sample has been electron irradiated and annealed twice in order to produce vacancy complexes. Please refer to the text for treatment details. The data for the 1.31 eV band (open symbols) were acquired at 100 K while the 1.68 eV data (solid symbols) were measured at 77 K. The uncertainties for the Raman-normalized PL intensity and silicon concentration measurements are both ±10%. The dashed lines are included to guide the eye of the reader.

increase after this treatment in the layers with higher silicon concentrations, as measured by SIMS. The intensity of the ZPL for the neutral (N-V) center, $(\text{N-V})^0$ (2.156 eV), was always measured to be 2 or 3 orders of magnitude greater than that for the negative charge state, $(\text{N-V})^-$ (1.945 eV), indicating that the sample layers contained low concentrations of nitrogen donors, N_S^0.[36–38]

IV. DISCUSSION

A. Vibronic structure of the 1.31 eV band

According to theory, the transition probability, and thus total integrated intensity, of a vibronic absorption band is temperature (T) independent for two energetically isolated electronic states.[39,40] However, the fraction of the transition probability in the ZPL decreases as the temperature is increased. Since the vibronic band shapes are uncertain in both PL and optical absorption, the temperature dependence of the ZPL will be parameterized using the well-known single, effective mode model.[39–42] The integrated absorption of the ZPL, A_{ZPL}, is thus given by

$$A_{\text{ZPL}}(T) \propto \exp[-S_{\text{HR}} \times \coth(\hbar\omega/2k_BT)] \times J_0[S_{\text{HR}} \times \text{csch}(\hbar\omega/2k_BT)], \quad (1)$$

where J_0 is a Bessel function, $\hbar$ is the reduced Planck's constant, and k_B is the Boltzmann constant.[40–42] The least-squares fit to the data, illustrated in Fig. 4, estimated that $S_{\text{HR}} \sim 1.5$ and $\hbar\omega \sim 28$ meV for the 1.31 eV optical band.

In Fig. 4 the fit to the temperature variation of the ZPL in absorption is superimposed on the PL data. For a simple two-level system the ZPL in PL and absorption is expected to have the same temperature dependence. Rather than decreasing in intensity as the temperature increased, the PL ZPL intensity showed a steady increase up to $T \sim 100$ K. This increase could be explained by including a nonradiative intermediate level between the ground and excited states of the 1.31 eV center which competes to trap the excited electrons.[40] A possible model is shown in Fig. 9, presenting some of the processes which may contribute to the 1.31 eV luminescence observed during 785-nm (1.58 eV) laser excitation. The photoconductivity measurements by Allers and Collins suggest that the ground state of the center attributed to the 1.31 eV ZPL is separated from a carrier band by approximately 1.5 eV.[35] For the proposed band diagrams in Figs. 9(a) and 9(b) the $(\text{Si-V})^0$ acceptor level is thus positioned ~1.5 eV above the valence band. The photoconductivity and temperature dependence of the PL data can be explained using these figures. In Fig. 9(a) direct optical excitation of an electron from the $^3A_{2g}$ ground state to the 1.31 eV excited state, followed by relaxation and de-excitation back to the ground state, results in emission of light with an energy of 1.31 eV. In Fig. 9(b) excitation of an electron from the valence band (producing a hole) to the excited states (the 1.31 eV state or the intermediate state, lying ΔE_t below the 1.31 eV state) is considered. As the temperature is increased the intermediate state may thermally populate the 1.31 eV state. Recombination between a hole in the valence band and an electron from the $^3A_{2g}$ ground state enables the de-excitation of the electron from the 1.31 eV state and the characteristic emission. The results presented in Fig. 4 suggest that the excited electrons are preferentially trapped by the nonradiative intermediate level with a higher probability than the 1.31 eV excited state. Assuming this model, the PL ZPL intensity is given by

$$I_{\text{ZPL}}(T) = C + [I(0)/(1 + g \times \exp(\Delta E_t/k_BT)] \times \exp[-S_{\text{HR}} \times \coth(\hbar\omega/2k_BT)] \times J_0[S_{\text{HR}} \times \text{csch}(\hbar\omega/2k_BT)], \quad (2)$$

where $I(0)$ is the intensity at $T = 0$ K, C is a constant to account for the possibility of direct excitation to the 1.31 eV level, g is the ratio of degeneracies of the trap and the 1.31 eV excited level, and ΔE_t is the energy separation between those states.[40] Fitting the data to Eq. (2) using S_{HR} and $\hbar\omega$ determined from the absorption data gives $\Delta E_t \sim 5$ meV, $1 \leqslant g \leqslant 3$, and $C/I(0) \sim 10^{-2}$. The fraction of the excitation leading to direct excitation of the 1.31 eV level is then $C/[C + I(0)/(1 + g)] \approx 0.02$ to 0.04. The trap state cannot be ^3E_u since the electronic dipole transition $^3A_{2g} \leftrightarrow {}^3E_u$ is allowed. However, candidate states include ^1E_g ($g = 1.5$) and $^1A_{1g}$ ($g = 3$)

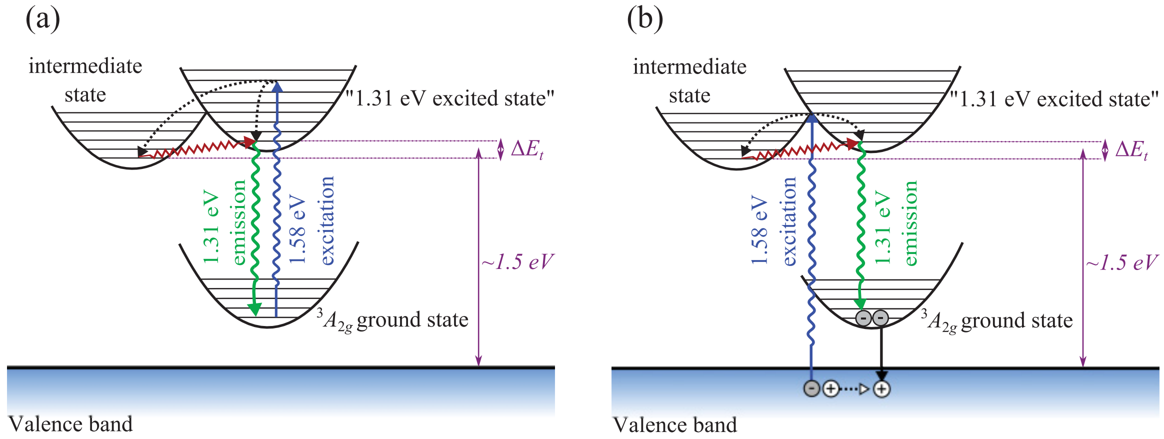

FIG. 9. (Color online) Schematic representation of the energy levels of (Si-V)^0 (not to scale) used to explain 1.31 eV emission and absorption. There is an allowed optical ZPL transition from the $^3A_{2g}$ ground state to the 1.31 eV excited state and an intermediate state ΔE_t below the 1.31 eV excited state to which optical transitions from the ground state are forbidden. The 1.31 eV ZPL emission could be excited using a 785-nm (1.58 eV) laser in two ways. (a) An electron is excited directly from the $^3A_{2g}$ ground state into the vibronic band of the 1.31 eV excited state. Relaxation to the bottom of the 1.31 eV excited state followed by emission is possible, but a nonradiative transition to the intermediate state could also occur. (b) Excitation of an electron from the valence band to the 1.31 eV excited or intermediate states and trapping of the resultant hole by the $^3A_{2g}$ ground state. Again, once the electron reaches the bottom of the excited state 1.31 eV ZPL emission is possible. In both cases, if the excited electron ends up in the intermediate state emission will not occur unless it is thermally excited into the 1.31 eV state, as illustrated by a zig-zag arrow.

from the configuration $a_{1g}^2 a_{2u}^2 e_u^4 e_g^2$, but other states cannot be ruled out. It is noteworthy that Allers and Collins observed a photoconductivity peak at 1.493 eV,[35] which is also present in Fig. 2(a). This may be associated with the intermediate state in Fig. 9. Nevertheless, from these results it is suggested that the filled $^3A_{2g}$ lies ~ 0.2 eV above the valence band.

B. Preferential alignment of (Si-V)^0

The (Si-V) center in diamond has D_{3d} symmetry. Therefore, the principal symmetry axis of the center can be aligned along four different directions: [111], $[\bar{1}\bar{1}1]$, $[1\bar{1}\bar{1}]$, and $[\bar{1}1\bar{1}]$. Consequently, if the (Si-V)^0 defects are randomly oriented over the four $\langle 111\rangle$ directions then the EPR spectrum produced by applying the magnetic field ($\boldsymbol{B}$) along any $\langle 111\rangle$ direction would consist of four groups ($n = 1,2,3,4$) of hyperfine (^{29}Si, ^{13}C) split lines. If the total integrated intensity of the nth group is I_n, then the relative integrated intensities I_1:I_2:I_3:I_4 would be 1:3:3:1, simply representing the fact that 1/4 of the defects have their symmetry axis parallel to the applied field, and for 3/4 the angle between the applied magnetic field and this axis is arccos(1/3). Figure 6(c) shows the low field half of the EPR spectrum, simulated using the published values for randomly oriented (Si-V)^0 centers and $R_{\langle 111\rangle} = I_2/I_1 = 3$, where the subscript on R indicates the direction of the magnetic field.[21] For a CVD diamond sample grown on a [110]-oriented substrate [i.e., growth on a (110) plane] two of the four $\langle 111\rangle$ directions lie in the (110) plane ($[1\bar{1}\bar{1}]$ and $[\bar{1}1\bar{1}]$) and two out of the (110) plane ([111] and $[\bar{1}\bar{1}1]$), as illustrated in Fig. 10. To parametrize the possible preferential orientation of (Si-V)^0 centers either "out of" or "in" the (110) plane it is useful to define the probability that a (Si-V)^0 defect is aligned along [111] as $p_{[111]} = \frac{p}{4}$, where $0 \leqslant p \leqslant 2$. Since the $[\bar{1}\bar{1}1]$ direction is equivalently "out of" the plane $p_{[\bar{1}\bar{1}1]} = \frac{p}{4}$. Then $p_{[\bar{1}1\bar{1}]} = p_{[1\bar{1}\bar{1}]} = \frac{2-p}{4}$. If $p = 1$, the (Si-V)^0 defects are randomly oriented over the four possible $\langle 111\rangle$ directions.

Thus, when $\boldsymbol{B}$ is along [111] or $[\bar{1}\bar{1}1]$,

$$R_{[111]} = R_{[\bar{1}\bar{1}1]} = \frac{4-p}{p}\left(=\frac{I_2}{I_1}\right), \qquad (3)$$

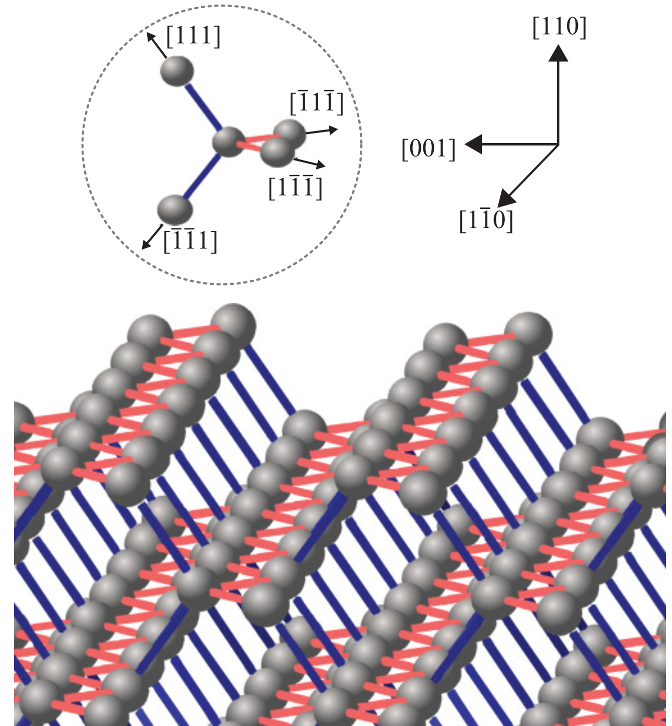

FIG. 10. (Color online) Cartoon of a view along a (110) growth plane, displaying the atomic scale roughness of the surface. Bonds that lie in the growth plane ($[\bar{1}1\bar{1}]$ and $[1\bar{1}\bar{1}]$) are shown in red and those that are out of the growth plane ([111] and $[\bar{1}\bar{1}1]$) are indicated by blue bonds.

TABLE II. Effective relative excitation rates for transitions for differently oriented trigonal defects, where $\phi = \arccos(1/\sqrt{3})$.

Defect Symmetry axis	$A_{2g} \leftrightarrow A_{1u}$ (D_{3d}) $A \leftrightarrow A$ (C_{3v})	$A_{2g} \leftrightarrow E_u$ (D_{3d}) $A \leftrightarrow E$ (C_{3v})
[111]	$\frac{1}{3}\cos^2(\alpha)$	$[\sin(\alpha) + \sqrt{\frac{2}{3}}\cos(\alpha)]^2$
$[\bar{1}\bar{1}1]$	$\frac{1}{3}\cos^2(\alpha)$	$[\sin(\alpha) + \sqrt{\frac{2}{3}}\cos(\alpha)]^2$
$[\bar{1}1\bar{1}]$	$\cos^2(\phi - \alpha)$	$\sin^2(\alpha - \phi)$
$[1\bar{1}\bar{1}]$	$\cos^2(\phi + \alpha)$	$\sin^2(\alpha + \phi)$

and for $\boldsymbol{B}$ along $[\bar{1}1\bar{1}]$ or $[1\bar{1}\bar{1}]$,

$$R_{[\bar{1}1\bar{1}]} = R_{[1\bar{1}\bar{1}]} = \frac{2+p}{2-p}\left(=\frac{I_2}{I_1}\right). \tag{4}$$

In the as-grown sample A, grown on a {110} substrate [assumed to be (110)], the measured values for $R_{[\bar{1}1\bar{1}]} = 7.3 \pm 0.1$ and $R_{[111]} = 1.6 \pm 0.1$ [see Figs. 6(a) and 6(b), respectively]. These yield a value of $p = 1.53 \pm 0.05$, showing that ~80% of the $(\text{Si-V})^0$ defects were oriented out of the growth plane (i.e., with the D_{3d} axis along [111] or $[\bar{1}\bar{1}1]$). A degree of preferential alignment of the $(\text{Si-V})^0$ centers in sample A was retained until it was annealed at 2000 °C, whereupon the $(\text{Si-V})^0$ concentration was halved and the centers were observed to be statistically aligned. Reorientation of the (Si-V) unit is not possible without dissociation, and so it can be inferred that the HPHT anneal resulted in dissociation of $(\text{Si-V})^0$ centers and formation of $(\text{Si-V})^0$, with the former process dominating.

An incorporation process during CVD synthesis which could account for the preferential alignment of $(\text{Si-V})^0$ in samples grown on {110}-oriented diamond substrates can be postulated. First, a silicon atom is incorporated in a substitutional site on the uppermost diamond layer. The presence of the silicon atom may reduce the probability of incorporating a carbon atom in the nearest neighboring site in the next layer, producing a vacant site. The subsequent layer might overgrow the center. The substitutional silicon atom will then relax into the split-vacancy configuration, with the D_{3d} symmetry axis pointing out of the growth plane. Similarly, other trigonal silicon-vacancy-type defects would be expected to show preferential alignment in diamonds grown on {110}-oriented substrates.[22] A consequence of this process is that all the $(\text{Si-V})^0$ centers are expected to be preferentially oriented. The fact that only ~ 80% of the $(\text{Si-V})^0$ centers are preferentially oriented out of the growth plane is probably due to the sample studied containing material that was not only the result of growth on a flat {110} surface. Roughening of the surface during growth, producing differently oriented microfacets, and material grown on the edge of the sample on different crystal faces would result in the reduced preferential orientation measured.

Sample B, which was grown on a {100}-oriented substrate, did not show any preferential alignment. This is understandable since the ⟨111⟩ directions all make the same angle relative to the direction perpendicular to the growth plane and are thus indistinguishable during growth.

The incorporation efficiency of $(\text{Si-V})^0$ centers appears to be significantly lower in samples grown on {001}- than on {110}-oriented substrates. Samples A and B were grown simultaneously, yet the $(\text{Si-V})^0$ concentration was five times greater in sample A.

Preferential orientation of defects can also influence the measured absorption and emission. For an individual trigonal defect the dipole moment of the allowed optical transition is either parallel ($A \to A$ transition) or perpendicular ($A \to E$ transition) to the trigonal axis. In an $A \to E$ transition, the x and y polarizations must have equal dipole moments, by symmetry. In an experiment where the optical excitation is incident along the [110] crystallographic direction, and the angle between the linearly polarized electric ($\boldsymbol{E}$) field vector of the light and [001] is α, then the effective relative excitation rates for $A \to A$ and $A \to E$ transitions for the differently oriented trigonal defects are given in Table II, and plotted out in Fig. 11.

It is clear that for an optical absorption measurement on an ensemble of defects, randomly oriented over the possible ⟨111⟩ directions, the optical excitation, and hence absorption, is independent of the polarization of the electric field vector of the light. However, if all the defects are oriented out of the plane (i.e., [111] and $[\bar{1}\bar{1}1]$), for an $A \to A$ ($A \to E$) transition the optical absorption will be weaker (stronger) than for the same number of defects randomly oriented over the possible orientations. For the three samples indicated in Fig. 7, the optical absorption measurements were made with the light incident along [110], and from EPR it was known that the $(\text{Si-V})^0$ defects were preferentially oriented along [111] and $[\bar{1}\bar{1}1]$. Assuming that 80% of the $(\text{Si-V})^0$ were oriented along [111] and $[\bar{1}\bar{1}1]$, and that the incident light was unpolarized, the optical absorption can be corrected to account for the preferential orientation. If the 1.31 eV $(\text{Si-V})^0$ transition is either ${}^3A_{2g} \to {}^3A_{1u}$ or ${}^3A_{2g} \to {}^3E_u$ it is apparent that these data points are only consistent with the correlation between the concentration of $(\text{Si-V})^0$ and the integrated intensity of the 1.31 eV optical absorption if the transition is between a ${}^3A_{2g}$ ground state and a ${}^3A_{1u}$ excited state.

The Raman-normalized PL spectrum in Fig. 3(a) is from an as-grown sample for which EPR measurements showed that the $(\text{Si-V})^0$ centers were preferentially oriented, at a concentration of 500 ± 70 ppb (1 ppb = 1 part per billion carbon atoms). After annealing at 2000 °C, the concentration decreased to 250 ± 20 ppb, with equally distributed orientations, and with little change to the Raman-normalized PL from the 1.31 eV line [Fig. 3(b)]. Correcting the intensities to allow for the effect of the anisotropic distribution on the excitation efficiency and on the luminescence, it is found that the intensity of the PL is approximately proportional to the $(\text{Si-V})^0$ concentration.

C. Charge transfer between 1.31 eV and 1.68 eV bands

The simultaneous presence of different charge states of the same defect in diamond is not uncommon. The relative concentrations of the charge states is determined by (a) the concentrations of other impurities which can act as acceptors or donors and (b) the treatment history such as photoexcitation or moderate heating (here defined as <800 °C). Using this method, the neutral and negative charge states of several

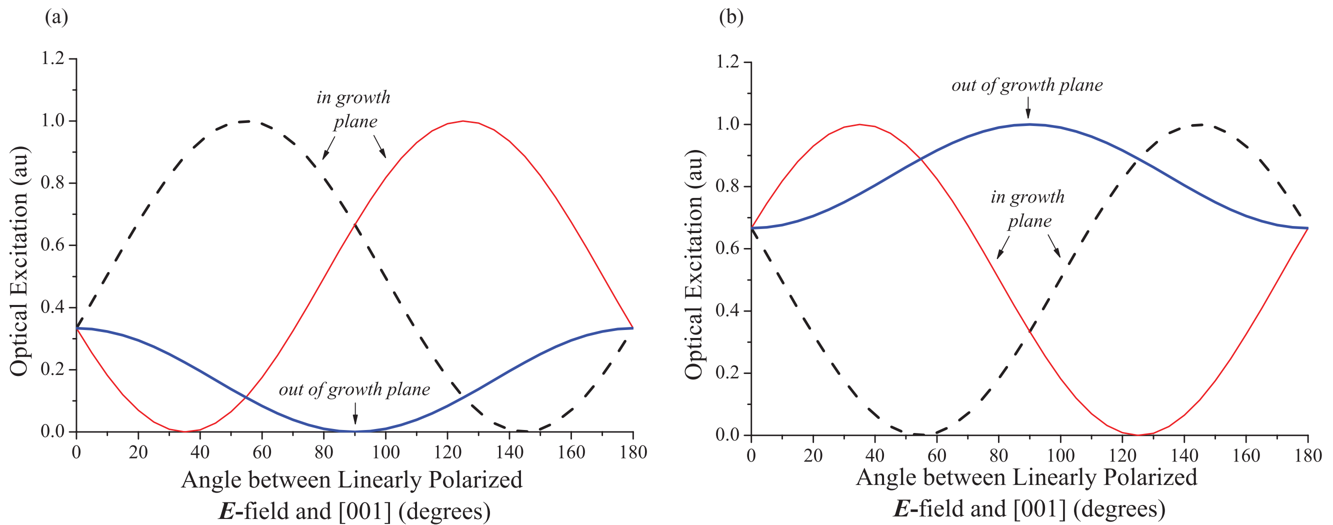

FIG. 11. (Color online) Theoretical polarization dependence of the optical excitation for trigonal defects with their symmetry axes aligned parallel to ⟨111⟩ directions lying in [dashed (black) and thin solid (red) curves] and out of [thick solid (blue) curve] the growth plane for CVD diamond grown on a {110}-oriented substrate for (a) an $A \rightarrow A$ transition and (b) an $A \rightarrow E$ transition.

defects in diamond have been studied, such as those of the vacancy ($V^{0/-}$, known as GR1 and ND1),[43,44] the di-nitrogen vacancy [$(N\text{-}V\text{-}N)^{0/-}$, known as H3 and H2],[45] the nitrogen-vacancy-hydrogen [$(N\text{-}V\text{-}H)^{0/-}$],[46,47] and the nitrogen-vacancy [$(N\text{-}V)^{0/-}$] centers.[48]

For the charge transfer experiments reported in Fig. 3 of Ref. 19, which used sample A after annealing at 2000 °C, heating in the dark resulted in an increase in the intensity of the 1.68 eV band and a decrease in that of the 1.31 eV band. This treatment also induced a decrease in the $N_S{}^0$ and $(Si\text{-}V)^0$ concentrations, as measured by EPR. The opposite effect could be generated by sample illumination with light of energy greater than the band gap. Photobleaching of the 1.68 eV ZPL has previously been observed for single centers in nanodiamond illuminated by a 671-nm (1.85 eV) frequency doubled DPSS laser.[16] The 1.68 eV band has previously been ascribed to either the $(Si\text{-}V)^-$ or $(Si\text{-}V)^0$ centers;[1,2,49] these results unambiguously show that the 1.68 eV band cannot be $(Si\text{-}V)^0$ as the change in intensity of the ZPL is opposite to that observed for the $(Si\text{-}V)^0$ concentration measured by EPR. Instead, the relative change in the intensity of the 1.31 eV band after the treatments matched the changes to the EPR concentration of $(Si\text{-}V)^0$. These results can be explained by assuming that the 1.31 eV and 1.68 eV bands arise from chemically indistinguishable sites, so that the 1.31 eV band is attributed to a transition from the ground state to an excited state at the $(Si\text{-}V)^0$ center. This is further supported by the correlation between the average $(Si\text{-}V)^0$ concentration measured by EPR and the integrated intensity of the 1.31 eV illustrated in Fig. 7.

Using this information it is possible to envisage a simplified model for the processes induced by the treatments. The positions of the ground states of the $N_S{}^0$ and $(Si\text{-}V)^0$ centers relative to the conduction and valence bands of diamond have been published. Measurements of the resistance as a function of temperature in diamonds doped with single substitutional nitrogen place the donor level for $N_S{}^0$ 1.7 eV below the bottom of the diamond conduction band.[50] For the proposed band diagram in Fig. 12 the $(Si\text{-}V)^0$ acceptor level is positioned ~1.5 eV above the top of the valence band, as discussed in Sec. IV A. When the samples are heated it is suggested that some of the charge from the $N_S{}^0$ impurities was transferred to the $(Si\text{-}V)^0$ centers, creating $(Si\text{-}V)^-$. However, the change in the $(Si\text{-}V)^0$ concentration was greater than that of the $N_S{}^0$ ($|\Delta[(Si\text{-}V)^0]| = 100 \pm 20$ ppb while $|\Delta[N_S{}^0]| = 19 \pm 1$ ppb for the 2000 °C annealed sample A, implying that electrons were also thermally excited directly into the $(Si\text{-}V)^0$ levels. Comparison of the energy separation between the $(Si\text{-}V)^0$ and $N_S{}^0$ levels to their closest carrier bands shows that this is an acceptable proposition. However, this requires that the resulting holes in the valence band were then filled by the loss of an electron from at least one other defect, here denoted T. Conversely, illuminating the samples excited electrons from the valence band into the conduction band, simultaneously creating holes in the former band, which could have stimulated transitions to and from gap states. Free holes could diffuse to $(Si\text{-}V)^-$ defects, converting $(Si\text{-}V)^-$ centers to $(Si\text{-}V)^0$ centers. Meanwhile, the electrons in the conduction band could be trapped by $N_S{}^+$ and T^0. This picture is highly simplified, as several of the capture processes will occur simultaneously for both treatments. However, their relative probabilities will be different for each treatment, such that the processes outlined for each case in Fig. 12 would dominate.

Unknown traps such as T have previously been invoked to explain charge transfer processes in CVD diamond, for instance, in the investigation of $(N\text{-}V\text{-}H)^{0/-}$ by Khan *et al.*[46] Interestingly, even for sample A, which was HPHT annealed, the existence of T was required in order to balance the charge transfer processes. An EPR or absorption feature which could be ascribed to T was not observed in the samples studied. However, this is unsurprising as the maximum concentration of T necessary to explain these results would be of the order of 100 ppb, which may be below our detection limit for this particular defect.

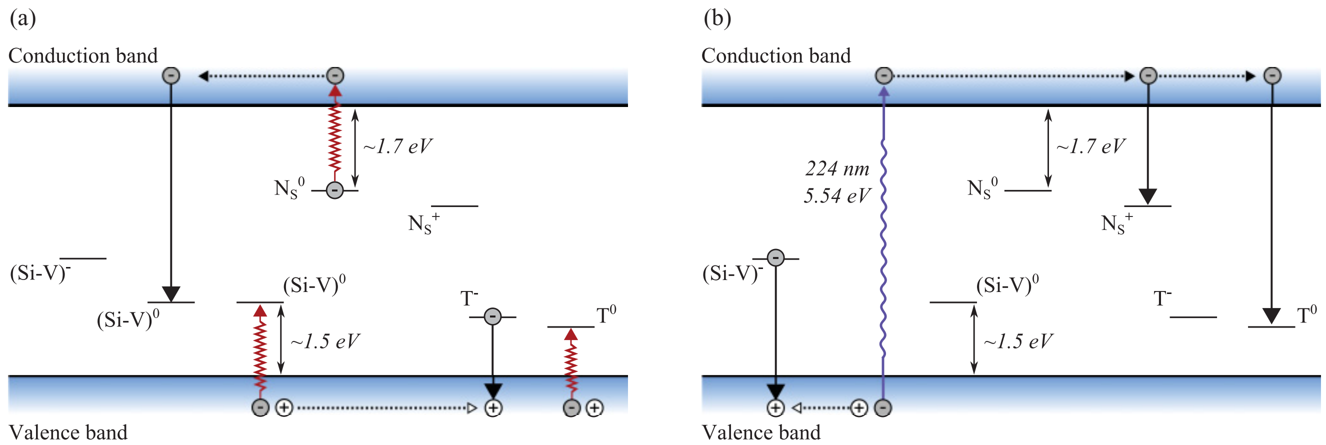

FIG. 12. (Color online) Schematic of the main phenomena occurring during the charge transfer process involving $(\text{Si-V})^0$, $(\text{Si-V})^-$, $N_S{}^0$, $N_S{}^+$, and the neutral and negative charge states of an unknown trap T. (a) When samples are heated for 20 min at 577 °C $(\text{Si-V})^0$ centers are converted to $(\text{Si-V})^-$ centers by two processes: Electrons are thermally released from the valence band to the $(\text{Si-V})^0$ acceptor levels, converting them into $(\text{Si-V})^-$ centers. Electrons are also thermally excited from the $N_S{}^0$ levels into the conduction band, from which they can de-excite into the $(\text{Si-V})^0$ level. Simultaneously, recombination between T^- and the holes in the valence band occurs. (b) Illuminating with light of energy equal to or greater than the band gap excites electrons from the valence band into the conduction band. The electrons can then migrate and de-excite into the $N_S{}^+$ and T^0 levels. Some of the holes which were consequently produced in the valence band trap electrons from the $(\text{Si-V})^-$ centers, increasing the $(\text{Si-V})^0$ concentration.

Optical absorption, like EPR, is a quantitative technique and the integrated intensity of a ZPL (in meV cm^{-1}) is often used to calculate the concentration of the center attributed to it (in cm^{-3}) using published calibration constants (in meV cm^2).[51] For diamond, it is standard to do the absorption measurements for defect concentration calculations at 77 K since cooling to this temperature is experimentally common and features are generally sharp, facilitating detection. From the linear correlation between the $(\text{Si-V})^0$ concentration and the integrated intensity of the absorption coefficient for the 1.31 eV band (Fig. 7) a calibration constant could be calculated,[22] giving

$$A_{1.31} = [1.6(\pm 0.3) \times 10^{-16}] \times [(\text{Si-V})^0]. \qquad (5)$$

Furthermore, by equating the change in the $(\text{Si-V})^0$ concentration to that of the $(\text{Si-V})^-$ centers during charge transfer and linking that to the change in the 1.68 eV ZPL integrated intensity a calibration equation for $(\text{Si-V})^-$ could also be determined:[22]

$$A_{1.68} = [3.6(\pm 0.7) \times 10^{-15}] \times [(\text{Si-V})^-]. \qquad (6)$$

The calibration constant for $(\text{Si-V})^0$ is similar to that for the $(\text{N-V})^-$ and V^0 (GR1) centers, which are $1.40(\pm 0.35) \times 10^{-16}$ meV cm^2 and $1.2(\pm 0.3) \times 10^{-16}$ meV cm^2,[32,51] respectively. Comparing Eqs. (5) and (6) suggests that the oscillator strength (which is proportional to the calibration constant) for $(\text{Si-V})^-$ is approximately 23 times larger than that for $(\text{Si-V})^0$. The factor of 23 could be partly accounted for by the difference in vibronic coupling. Taking the Huang-Rhys factor for the 1.68 eV band as 0.24,[16,17] and the 1.31 eV band as 1.5 (determined in this work) it is possible to account for a factor of ~4. The expression derived by detailed balance for the integrated absorption implies that a factor of ~2 can be attributed to the difference in energies.[39] This then requires only a difference in radiative lifetimes of ~3 [shorter for $(\text{Si-V})^-$] in order to account for the factor of 23.

D. Electron irradiation and annealing studies

At room temperature vacancies are immobile in diamond. Upon annealing at temperatures $\gtrsim 600\,°\text{C}$ the vacancies diffuse through the lattice.[32] In type IIa diamond the annealing of isolated vacancies (V) typically is described by mixed first- and second-order kinetics, $d[\text{V}]/dt = -r_1[\text{V}] - r_2[\text{V}]^2$, where [V] is the concentration of the vacancies, t is the time, and r_1 and r_2 are the rate constants for a specific annealing temperature. The first term represents the loss of vacancies to nonsaturable traps (e.g., surfaces and dislocations) and the second term accounts for the formation of divacancies, which are stable to ~800 °C.[52]

Substitutional nitrogen centers (N_S) are known to be effective traps for vacancies in diamond.[53] The relative intensities of the ZPLs for the neutral (2.156 eV) and negative (1.945 eV) charge states of the nitrogen-vacancy centers suggest that sample D contained a low concentration of $N_S{}^0$ donors and (N-V) centers.[38] It is thus reasonable to assume that silicon, which is the dominant dopant, and its complexes will be the principal traps for the vacancies created and mobilized during the irradiation and annealing treatments. The divacancy was ignored in the modeling of irradiation damage and annealing, given that the divacancy anneals out at the annealing temperature used and the significant concentration of traps for isolated vacancies present. Isolated self-interstitials[54] anneal out at temperatures ~550 °C and although a variety of interstitial complexes have been identified in type IIa diamond[55,56] there is no evidence for the interaction of self-interstitials with silicon. Thus, for this analysis self-interstitials were also ignored. Furthermore, due to the low substitutional nitrogen concentration, the treatments will primarily produce silicon-vacancy complexes in the neutral charge state. In as-grown

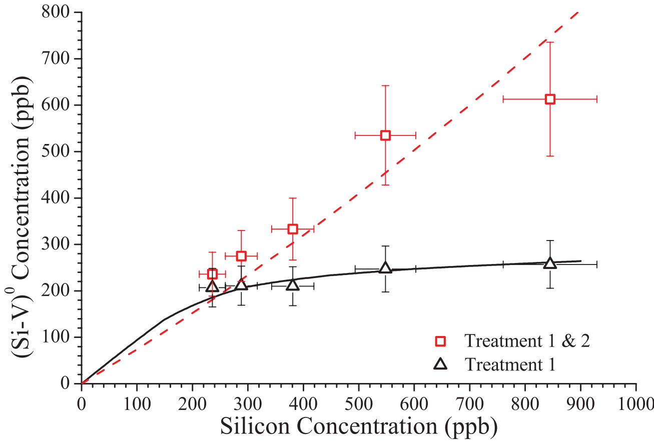

FIG. 13. (Color online) $(\text{Si-V})^0$ concentration in the different layers of sample D after electron irradiation and annealing treatments 1 and 2 (Table I). The lines indicate the simulated behavior when the system is modeled to include the loss of vacancies to dislocations and the formation (and destruction) of (Si-V) and (Si-V_2) centers via the reactions $\text{Si} + \text{V} \rightarrow (\text{Si-V})$ and $(\text{Si-V}) + \text{V} \rightarrow (\text{Si-V}_2)$.

material comparison of the EPR determined concentration of $(\text{Si-V})^0$, plus the optically determined concentration of $(\text{Si-V})^-$ (Sec. IV C), and SIMS measurements of the total silicon concentration indicate that typically only a fraction ($\lesssim 15\%$) of the silicon is accounted for in (Si-V) defects. The bulk of the silicon is presumed to be incorporated as substitutional silicon impurities (Si_S). Both (Si-V) and silicon divacancy, (Si-V_2), centers are expected to form according to $\text{Si}_\text{S} + \text{V} \rightarrow (\text{Si-V})$ and $(\text{Si-V}) + \text{V} \rightarrow (\text{Si-V}_2)$.[31] The kinetics of the system during isothermal annealing may therefore be described by

$$\frac{d[\text{V}]}{dt} = -r_1[\text{V}] - r_2[\text{Si}_\text{S}][\text{V}] - r_3[(\text{Si-V})][\text{V}], \quad (7)$$

$$\frac{d[\text{Si}_\text{S}]}{dt} = -r_2[\text{Si}_\text{S}][\text{V}], \quad (8)$$

$$\frac{d[(\text{Si-V})]}{dt} = r_2[\text{Si}_\text{S}][\text{V}] - r_3[(\text{Si-V})][\text{V}], \quad (9)$$

$$\frac{d[(\text{Si-V}_2)]}{dt} = r_3[(\text{Si-V})][\text{V}]. \quad (10)$$

Twitchen *et al.* determined that the vacancy production rate for irradiation of diamond with 1.9 MeV electrons at nominally room temperature was $\sim 0.5\ \text{cm}^{-1}$.[52] Lawson *et al.* derived a value of $0.6\ \text{cm}^{-1}$ for 2 MeV electrons[57] and Collins and Dahwich $0.7\ \text{cm}^{-1}$ for 3 MeV electrons[58] for diamond with low concentrations of nitrogen. The fit in Fig. 13 assumes a vacancy production rate of $\sim 0.44\ \text{cm}^{-1}$ for 1.5 MeV electrons at room temperature, a value that is not out of line with other results.

The intensity of the 1.31 eV and 1.68 eV bands across all layers of sample D increased dramatically after the first treatment, and the resulting $(\text{Si-V})^0$ concentration was approximately constant. For the subsequent treatment the electron irradiation dose was increased fivefold and the intensity of the 1.31 eV ZPL was observed to increase further in the layers containing high concentrations of silicon. However, the strength of the ZPL did not change (within error) in the layers containing low concentrations of silicon (~ 250 ppb). It was assumed that all the available substitutional silicon impurities had formed silicon-vacancy complexes after the first treatment (i.e., ~ 250 ppb) and that the Raman-normalized 1.31 eV ZPL PL intensity is proportional to the $(\text{Si-V})^0$ concentration. It was thus possible to estimate the $(\text{Si-V})^0$ concentration from the PL data, as illustrated in Fig. 13. This calibration is consistent with the PL measurements of other silicon-doped samples containing known concentrations of $(\text{Si-V})^0$ defects.

Using these assumptions it was possible to model the system upon annealing at 900 °C by numerically solving the coupled differential Eqs. (7)–(10). The rate constant for the first-order loss of vacancies was determined from the data of Davies *et al.* in type IIa diamond and not varied.[32] The only variable parameters were r_2 and r_3. The best fits to the data, shown by the lines in Fig. 13, were achieved with $r_1 = 4.40\ \text{h}^{-1}$, $r_2 = 0.11\ \text{ppb}^{-1}\text{h}^{-1}$, and $r_3 = 10^{-3}\ \text{ppb}^{-1}\text{h}^{-1}$. The value of r_2, and the data in Fig. 13 indicated that Si_S is an excellent trap for vacancies. (Si-V_2) is predicted to be stable at the annealing temperatures,[31] but the production is vacancy limited. The analysis predicts that further irradiation and annealing could produce substantial quantities of (Si-V_2).

V. CONCLUSIONS

The 1.31 eV system is identified with the $(\text{Si-V})^0$ center in diamond. The 1.31 eV ZPL shifts in energy when the silicon isotope is changed, conclusively identifying the center as silicon related. The electronic structure and vibronic coupling in the 1.31 eV band has been studied and the Huang-Rhys factor is ~ 1.5. A trapping level has been identified ~ 5 meV below the excited state involved in the 1.31 eV ZPL. The $(\text{Si-V})^0$ concentration determined by EPR has been shown to correlate with the integrated absorption of the 1.31 eV ZPL. This, combined with the analysis of charge transfer between $(\text{Si-V})^-$ (1.68 eV system) and $(\text{Si-V})^0$ has enabled the calculation of calibration constants relating the integrated absorption of the 1.68 eV and 1.31 eV ZPLs with the $(\text{Si-V})^-$ and $(\text{Si-V})^0$ defect concentrations, respectively.

$(\text{Si-V})^0$ defects have been shown to predominantly grow into CVD diamond as complete units, rather than being produced by the migration of vacancies which are trapped at substitutional silicon impurities. This results in the preferential alignment of the $(\text{Si-V})^0$ centers for homoepitaxial CVD on {110}-oriented substrates, with the D_{3d} symmetry axis pointing out of the growth plane. The reduction of the number of possible orientations of this defect from four to two could be useful in applications where their optical emission is coupled out of the diamond. It is important to correct for the preferential alignment of $(\text{Si-V})^0$ in the quantitative analysis of EPR and optical spectroscopic measurements. The preferential orientation has been utilized in polarized spectroscopic studies to identify the 1.31 eV ZPL as a transition between the $^3A_{2g}$ ground state and $^3A_{1u}$ excited states of $(\text{Si-V})^0$.

No evidence for quenching of the 1.31 eV band in PL has been detected, even though a variety of previously unreported probably silicon-related optical centers have been

observed, allowing semiquantitative analysis of PL data. SIMS measurements show that only a fraction of the incorporated silicon impurities in as-grown CVD diamond is in the form of (Si-V) defects, the majority being substitutional silicon atoms. Irradiation and annealing at temperatures where vacancies are mobile dramatically increases the concentration of (Si-V) defects; substitutional silicon appears to be a very effective trap for vacancies. Modeling of the experimental data on the production of (Si-V) in irradiated silicon-doped diamond suggests that substantial quantities of (Si-V_2) can be produced if sufficient concentrations of vacancies are introduced.

ACKNOWLEDGMENTS

Dave Evans and Samantha Sibley (DTC Research Centre, Maidenhead) and Chris Kelly (Element Six) are thanked for their help with sample preparation and characterization. U.F.S.D.-J. thanks the DTC Research Centre for an Industrial Bursary. We acknowledge funding from the Engineering and Physical Sciences Research Council and Birmingham Science City: Innovative Uses for Advanced Materials in the Modern World (West Midlands Centre for Advanced Materials 1 and 2), supported by Advantage West Midlands and partly funded by the European Regional Development Fund.

*m.e.newton@warwick.ac.uk

[1] C. D. Clark, H. Kanda, I. Kiflawi, and G. Sittas, Phys. Rev. B **51**, 16681 (1995).
[2] J. P. Goss, R. Jones, S. J. Breuer, P. R. Briddon, and S. Öberg, Phys. Rev. Lett. **77**, 3041 (1996).
[3] J. Barjon, E. Rzepka, F. Jomard, J. M. Laroche, D. Ballutaud, T. Kociniewski, and J. Chevallier, Phys. Status Solidi A **202**, 2177 (2005).
[4] L. H. Robins, L. P. Cook, E. N. Farabaugh, and A. Feldman, Phys. Rev. B **39**, 13367 (1989).
[5] S. D. Williams, D. J. Twitchen, P. M. Martineau, G. A. Scarsbrook, and I. Friel, "High colour diamond," UK Patent GB2428690 B (2010).
[6] H. Kanda and T. Sekine, in *Properties and Growth of Diamond*, 1st ed., EMIS Data Review Series No. 9, edited by G. Davies (INSPEC, London, 1994), Chap. 12, pp. 405–408.
[7] C. M. Breeding and W. Wang, Diam. Relat. Mater. **17**, 1335 (2008).
[8] W. Wang (private communication, 2011).
[9] A. Beveratos, S. Kühn, R. Brouri, T. Gacoin, J.-P. Poizat, and P. Grangier, Eur. Phys. J. D **18**, 191 (2002).
[10] F. Jelezko and J. Wrachtrup, Phys. Status Solidi A **203**, 3207 (2006).
[11] T. Gaebel, I. Popa, A. Gruber, M. Domhan, F. Jelezko, and J. Wrachtrup, New J. Phys. **6**, 98 (2004).
[12] E. Wu, J. R. Rabeau, G. Roger, F. Treussart, H. Zeng, P. Grangier, S. Prawer, and J.-F. Roch, New J. Phys. **9**, 434 (2007).
[13] I. Aharonovich, S. Castelletto, D. A. Simpson, A. D. Greentree, and S. Prawer, Phys. Rev. A **81**, 043813 (2010).
[14] G. Balasubramanian, P. Neumann, D. Twitchen, M. Markham, R. Kolesov, N. Mizuochi, J. Isoya, J. Achard, J. Beck, J. Tissler, V. Jacques, P. R. Hemmer, F. Jelezko, and J. Wrachtrup, Nat. Mater. **8**, 383 (2009).
[15] C. L. Wang, C. Kurtsiefer, H. Weinfurter, and B. Burchard, J. Phys. B **39**, 37 (2006).
[16] E. Neu, D. Steinmetz, J. Riedrich-Möller, S. Gsell, M. Fischer, M. Schreck, and C. Becher, New J. Phys. **13**, 025012 (2011).
[17] A. T. Collins, L. Allers, C. J. Wort, and G. A. Scarsbrook, Diam. Relat. Mater. **3**, 932 (1994).
[18] A. A. Gorokhovsky, A. V. Turukhin, R. R. Alfano, and W. Phillips, Appl. Phys. Lett. **66**, 43 (1995).
[19] K. Iakoubovskii, G. J. Adriaenssens, N. N. Dogadkin, and A. A. Shiryaev, Diam. Relat. Mater. **10**, 18 (2001).
[20] K. Iakoubovskii, A. Stesmans, B. Nouwen, and G. J. Adriaenssens, Phys. Rev. B **62**, 16587 (2000).
[21] A. M. Edmonds, M. E. Newton, P. M. Martineau, D. J. Twitchen, and S. D. Williams, Phys. Rev. B **77**, 245205 (2008).
[22] U. F. S. D'Haenens-Johansson, A. M. Edmonds, M. E. Newton, J. P. Goss, P. Briddon, J. M. Baker, P. M. Martineau, R. U. A. Khan, D. J. Twitchen, and S. D. Williams, Phys. Rev. B **82**, 155205 (2010).
[23] B. J. Masters, Solid State Commun. **9**, 283 (1971).
[24] J. P. Goss, P. R. Briddon, R. Jones, and S. Sque, Diam. Relat. Mater. **13**, 684 (2004).
[25] V. A. Nadolinny, A. P. Yelisseyev, O. P. Yuryeva, and B. N. Feygelson, Appl. Magn. Reson. **12**, 543 (1997).
[26] V. A. Nadolinny, A. P. Yelisseyev, J. M. Baker, M. E. Newton, D. J. Twitchen, S. C. Lawson, O. P. Yuryeva, and B. N. Feigelson, Journal of Physics-Condensed Matter **11**, 7357 (1999).
[27] R. Larico, J. Justo, W. Machado, and L. Assali, Physica B **376-377**, 292 (2006).
[28] L. Assali, W. Machado, R. Larico, and J. Justo, Diam. Relat. Mater. **16**, 819 (2007).
[29] G. D. Watkins, Phys. Rev. B **12**, 4383 (1975).
[30] C. A. Coulson and F. P. Larkins, J. Phys. Chem. Solids **30**, 1963 (1969).
[31] J. P. Goss, P. R. Briddon, and M. J. Shaw, Phys. Rev. B **76**, 075204 (2007).
[32] G. Davies, S. C. Lawson, A. T. Collins, A. Mainwood, and S. J. Sharp, Phys. Rev. B **46**, 13157 (1992).
[33] D. F. Howarth, J. A. Weil, and Z. Zimpel, J. Magn. Reson. **161**, 215 (2003).
[34] C. D. Clark, J. Phys. Chem. Solids **8**, 481 (1959).
[35] L. Allers and A. T. Collins, J. Appl. Phys. **77**, 3879 (1995).
[36] G. Davies, J. Phys. C **12**, 2551 (1979).
[37] G. Davies and M. F. Hamer, Proc. R. Soc. London A **348**, 285 (1976).
[38] A. T. Collins, J. Phys. Condens. Matter **14**, 3743 (2002).
[39] G. Davies, Semicond. Semimet. **51**, 1 (1998).
[40] G. Davies, Rep. Prog. Phys. **44**, 787 (1981).
[41] K. Huang and A. Rhys, Proc. R. Soc. A **204**, 406 (1950).
[42] K. K. Rebane, *Impurity Spectra of Solids: Elementary Theory of Vibrational Structure* (Plenum Press, New York, 1970).
[43] H. B. Dyer and L. D. du Preez, J. Chem. Phys. **42**, 1898 (1965).
[44] A. T. Collins and S. Rafique, Proc. R. Soc. A **367**, 81 (1979).
[45] Y. Mita, Y. Nisida, K. Suito, A. Onodera, and S. Yazu, J. Phys. Condens. Matter **2**, 8567 (1990).
[46] R. U. A. Khan, P. M. Martineau, B. L. Cann, M. E. Newton, and D. J. Twitchen, J. Phys. Condens. Matter **21**, 364214 (2009).
[47] R. U. A. Khan, P. M. Martineau, B. L. Cann, M. E. Newton, H. K. Dhillon, and D. J. Twitchen, Gems. Gemol. **46**, 18 (2010).
[48] N. Manson and J. Harrison, Diam. Relat. Mater. **14**, 1705 (2005).

[49]K. Iakoubovskii, G. J. Adriaenssens, and M. Nésladek, J. Phys. Condens. Matter **12**, 189 (2000).
[50]R. G. Farrer, Solid State Commun. **7**, 685 (1969).
[51]G. Davies, Physica B **274**, 15 (1999).
[52]D. J. Twitchen, M. E. Newton, J. M. Baker, T. R. Anthony, and W. F. Banholzer, Phys. Rev. B **59**, 12900 (1999).
[53]A. T. Collins, J. Phys. C **13**, 2641 (1980).
[54]D. C. Hunt, D. J. Twitchen, M. E. Newton, J. M. Baker, J. K. Kirui, J. A. van Wyk, T. R. Anthony, and W. F. Banholzer, Phys. Rev. B **62**, 6587 (2000).
[55]D. C. Hunt, D. J. Twitchen, M. E. Newton, J. M. Baker, T. R. Anthony, W. F. Banholzer, and S. S. Vagarali, Phys. Rev. B **61**, 3863 (2000).
[56]D. J. Twitchen, M. E. Newton, J. M. Baker, O. D. Tucker, T. R. Anthony, and W. F. Banholzer, Phys. Rev. B **54**, 6988 (1996).
[57]S. C. Lawson, D. Fisher, D. C. Hunt, and M. E. Newton, J. Phys. Condens. Matter **10**, 6171 (1998).
[58]A. T. Collins and A. Dahwich, J. Phys. Condens. Matter **15**, L591 (2003).